Applied Catalysis B: Environmental 163 (2015) 487–498

Contents lists available at ScienceDirect

Applied Catalysis B: Environmental

journal homepage: www.elsevier.com/locate/apcatb

Fe/HY zeolite as an effective catalyst for levulinic acid production from glucose: Characterization and catalytic performance

Nur Aainaa Syahirah Ramli, Nor Aishah Saidina Amin*

Chemical Reaction Engineering Group (CREG), Energy Research Alliance, Faculty of Chemical Engineering, Universiti Teknologi Malaysia, 81310 UTM Johor, Johor Bahru, Malaysia

ARTICLE INFO

Article history:
Received 15 May 2014
Received in revised form 22 July 2014
Accepted 19 August 2014
Available online 27 August 2014

Keywords:
Levulinic acid
Fe/HY zeolite catalyst
Acidity
Porosity
Biomass conversion

ABSTRACT

A series of Fe/HY zeolite catalysts with different $FeCl_3$ weight percent (5, 10 and 15%) on HY zeolite have been synthesized in this study. All the catalysts were characterized by XRD, FESEM, N_2 physisorption, FTIR, TGA, NH_3-TPD and IR-pyridine. The performance of the Fe/HY catalysts was tested in glucose to levulinic acid transformation. The amount and type of acid sites together with surface area and porosity influenced the catalytic activity. The catalyst with a large surface area, high concentration of active acid sites and appropriate ratio of Brønsted to Lewis acids seemed suitable for levulinic acid production. However, catalyst with excess Lewis acidity converted glucose into humins, but samples with high relative mesopority and low relative microporosity gave a decent levulinic acid yield. Among the catalysts tested, 10% Fe/HY catalyst exhibited the highest catalytic performance with 62% yield at 180 °C in 180 min. The reused catalyst exhibited constant activity for five successive runs. The experimental results demonstrated the potential of Fe/HY catalyst for biomass conversion to levulinic acid under mild process conditions.

1. Introduction

The depletion and price hike of fossil fuel resources have exacerbated the utilization of renewable sources such as biomass for the production of energy [1]. Currently, extensive research are being carried out to investigate the conversion of biomass into biofuels and other chemical feedstocks [2,3]. C_6 sugars (e.g. glucose and fructose) have been used as feedstocks to produce 5-hydroxymethylfurfural (HMF) and levulinic acid. The formation of HMF, an intermediate product for levulinic acid production, is proposed to take place through the dehydration of a five-membered ring monosaccharide. Therefore, fructose can be easily converted into HMF and levulinic acid in aqueous solution.

Levulinic acid is a versatile building block containing a ketone carbonyl group and an acidic carboxyl group. Levulinic acid can be used for the preparation of various high value-added organic chemicals, polymers, resin, flavor substances and fuel additives with numerous potential industrial applications [4]. Esterification of levulinic acid with alcohols produces levulinic esters for diesel additives [5]. Levulinic acid can also undergo hydrogenation to produce γ-valerolactone (GVL), to be blended with gasoline as well as to serve as a precursor of polymers and fine chemicals [6]. The first commercial-scale plant for the synthesis of levulinic acid from biomass was built in Caserta, Italy, through a process developed by Biofine Renewables [7,8]. The Biofine process involves two different stages of acid-catalyzed hydrolysis for the optimum product yield and minimum product degradation and tar formation [7]. The first stage is the fast production of HMF in only few seconds, while the production of levulinic acid in the second stage requires longer residence time.

Although glucose is less reactive in dehydration compared to fructose due to its comparatively stable nature, it is more preferable since glucose is less expensive. Initially, acids (H_2SO_4, HCl, formic acid) have been used as homogeneous catalysts for the production of levulinic acid from various feedstocks including fructose, glucose, cellulose and lignocellulosic biomass [9–11]. The homogeneous catalytic system is effective, but caused several problems such as equipment corrosion, environmental pollution and acid recycling. As an alternative, heterogeneous catalyst is introduced to overcome the problems associated with homogeneous catalytic system. Generally, solid acid catalysts used for the production of levulinic acid are reusable, with tolerable reduction in product yield until five to six runs [12,13]. Consequently, equipment corrosiveness and cost required for the overall process will be less in a heterogeneous system.

* Corresponding author. Tel.: +60 75535579; fax: +60 75588166.
E-mail addresses: noraishah@cheme.utm.my, profnoraishah@yahoo.com (N.A.S. Amin).

http://dx.doi.org/10.1016/j.apcatb.2014.08.031
0926-3373/

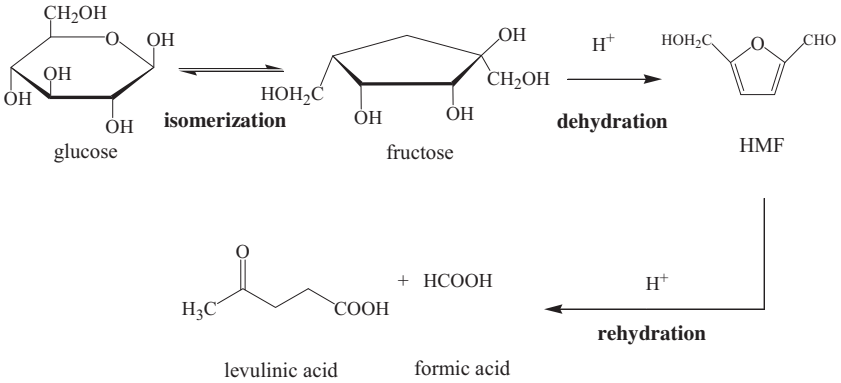

Fig. 1. Reaction scheme of glucose conversion to levulinic acid.

Since solid catalysts are preferred over homogeneous acid catalysts, numerous studies have been conducted for the synthesis of levulinic acid using various feedstocks [1,12–17]. The solid catalysts include zeolites, metal halides, nafion, $S_2O_8^{2-}/ZrO_2–SiO_2–Sm_2O_3$ solid superacid, niobium phosphate and clay. Previously, zeolite solid acids such as ZSM-5, LZY and MFI type zeolites have been tested as catalysts for levulinic acid production [18–21]. Zeolites have good potential to be used in glucose dehydration since the pore structures exert significant influence on the reaction [20,22,23]. At prolonged reaction time (8–15 h), 43, 20 and 36% levulinic acid yield were produced from fructose and glucose at reaction temperature 140–180 °C [18–20]. These reactions required 140 °C and 15 h of reaction temperature and time, respectively, for fructose conversion [18] while for glucose conversion to levulinic acid the temperature and time were 160 °C, 10 h for one study [19] and 180 °C, 8 h for another [20]. It is apparent that less reaction time is required if reaction temperature is higher.

Several studies have reported that some metal salts can hydrolyze carbohydrates effectively into useful feedstock chemicals. Peng et al. [13] applied metal chlorides as the catalyst for cellulose hydrolysis to levulinic acid and found that these metal chlorides enhanced the levulinic acid production in a shorter reaction time, but higher reaction temperatures were required. Earlier researchers mostly used $CrCl_2$ or $CrCl_3$ as the catalyst for catalytic conversion of glucose [13,24–26]. However, high price, toxicity and environmental pollution have necessitated the search for a non-toxic and low-cost hydrolysis catalyst. Instead of using Cr, other metal chlorides can be considered for the catalytic conversion of glucose. Therefore, further studies are warranted to discover more reactive catalysts for levulinic acid production at adequate process conditions. These can be done through testing the catalytic performance and investigating the physicochemical properties. Due to the low cost and non-toxic properties of $FeCl_3$ [27], it is envisaged that this extensively available compound is able to perform as an eco-friendly catalyst for levulinic acid production from glucose.

Catalytic performance testing over several types of zeolite revealed that the properties of solid catalyst, including the amount and strength of acid sites, types of acid sites, porosity and shape selectivity have significant effect on the yield and selectivity of levulinic acid [28]. Basically, in the conversion of glucose to levulinic acid, glucose isomerizes to fructose and dehydrates to form the intermediate product, HMF, which will then catalytically rehydrate to form levulinic acid and formic acid by hydronium ions [13,19]. The glucose conversion reaction scheme to levulinic acid is shown in Fig. 1. The isomerization of glucose to fructose is catalyzed by the Lewis acid sites [29]. Both Lewis and Brønsted acid sites are required for dehydration reaction, while Brønsted acid sites are required for HMF rehydration to levulinic acid. Besides, Lewis acid sites can also catalyzed decomposition of glucose to form humins [28,29]. By using zeolite and metal halide alone as catalyst, low levulinic acid yield has been reported in literatures [13,30,31]. This condition occurred probably because the intermediate compound, HMF, did not undergo ring cleavage to form linear-type molecules—levulinic acid and formic acid [32]. In addition, low acidity and porosity of the catalyst could also be the reason behind the low activity. Thus, modification of porous zeolite catalyst with acidic metal halide to form a new catalyst might improve the catalytic properties and enhance the levulinic acid production at adequate process conditions. Metal-modified zeolite catalysts may point toward higher catalytic activity than other types of acid catalysts and could be easily separated from the reaction products.

There are only few reports available on modified zeolite-catalyzing levulinic acid production from glucose [32]. Thus, we employed a series of modified Fe/HY zeolite prepared by impregnation of various amount of $FeCl_3$ on HY zeolite in this study. The properties of Fe/HY zeolite and parent catalyst (HY zeolite) were meticulously characterized via XRD, FESEM, N_2 physisorption, FTIR, TGA, NH_3-TPD and IR-pyridine. The relationship of physicochemical properties and catalytic activity in the production of levulinic acid were examined. The leaching of Fe ions, reusability of Fe/HY zeolite catalyst and its properties were also addressed in this study.

2. Experimental

2.1. Materials

NaY faujasite-type zeolite ($SiO_2/Al_2O_3 = 5$) was purchased from Zeolyst International Inc. Iron chloride ($FeCl_3$), 3,5-dinitrosalicylic acid and D-glucose were supplied by Merck, Germany. Potassium sodium tartrate tetrahydrate and sodium hydroxide (NaOH) were acquired from Sigma Aldrich, USA. Sulfuric acid (H_2SO_4), sodium sulfite and ammonium chloride (NH_4Cl) were obtained from QRec, New Zealand. A standard analytical grade of levulinic acid 98% (Merck), 5-hydroxymethylfurfural (HMF) 99% (Sigma Aldrich) and formic acid 99% (Merck) were used for the analysis of the products. Distilled water was used in all reaction solutions.

2.2. Catalyst preparation

HY zeolite was prepared by exchanging the ion from NaY zeolite with NH_4Cl. NaY zeolite was contacted with 2 M of NH_4Cl with stirring at room temperature for 2 h. The precipitate was then washed with distilled water, followed by drying overnight at 120 °C. The material was calcined at 500 °C for 5 h, resulting in the HY zeolite. Fe/HY zeolite catalysts were prepared by wetness impregnation method. Samples with different $FeCl_3$ to HY zeolite weight ratios (5, 10, 15 wt%) are identified as 5% Fe/HY, 10% Fe/HY and 15% Fe/HY catalysts in this study. $FeCl_3$ solution and HY zeolite powder with

certain weight ratio of $FeCl_3$ to zeolite were mixed and stirred at room temperature for 2 h. Then, the mixture was dried in the oven overnight at 120 °C. Finally, the Fe/HY zeolite catalyst was calcined at 400 °C for 5 h.

2.3. Catalyst characterization

Powder X-ray diffraction (XRD) of the catalysts was evaluated using a Bruker D8 advance diffractometer system (Cu Kα radiation, 40 kV, 30 mA) and the 2θ angle between 5 and 80°. The average crystallite size was determined using the Scherrer equation (Eq. (1)).

$$D = \frac{k\lambda}{\beta \cos\theta} \quad (1)$$

where k is a constant (0.98), λ is X-ray wavelength (1.54178 Å), β is the full peak width at half maximum in radian of the most intense diffraction peak position and θ is the Bragg's angle of the 2θ peak. The morphology and elemental analysis of the Fe/HY zeolite catalyst samples were observed by field emission scanning electron microscopy with energy-dispersive X-ray spectrometry (FESEM-EDX; Hitachi SU8020).

The surface area, pore size and volume of catalyst samples were evaluated according to the standard N_2 physisorption using a Micromeritics ASAP2020 analyzer. The catalyst samples were outgassed in vacuum at 100 °C before N_2 physisorption. The surface area of the catalyst samples was determined using Brunauer–Emmet–Teller (BET) method. The distributions of the micropores and mesopores were estimated by the *t*-plot and Barrett, Joyner & Halenda (BJH) methods, respectively. Meanwhile, for the analysis of the structure, Fourier-transformed infrared spectroscopy (FTIR) spectra of catalyst samples were obtained from powdered samples on KBr pellets using a Perkin-Elmer spectrum with a resolution of 4 cm^{-1} in the 4500–400 cm^{-1} of IR range. Thermal gravimetric analyses (TGA) were conducted using a TGA instrument (Netzsch STA 449 F3 Jupiter). About 10 mg of the catalyst sample was placed in a platinum pan and heated from 30 to 800 °C under N_2 flow at a heating rate of 10 °C/min.

The acid properties of the catalyst samples were determined using temperature-programmed desorption (TPDRO 1100 series, Thermo Finnigin) with ammonia as the probe molecule (NH_3-TPD). Initially, a catalyst sample (500 mg) was degassed at 150 °C for 0.5 h under a constant nitrogen flow (20 ml/min). Then, the sample was cooled to 50 °C and ammonia was adsorbed for 1 h. After saturation, nitrogen was purged for 0.5 h at 20 ml/min to remove excess ammonia on the catalyst surface. Finally, the catalyst sample was heated from 50 to 800 °C under a constant helium flow (20 ml/min). The concentration of desorbed ammonia was quantified by a thermal conductivity detector (TCD). The Brønsted and Lewis acid sites of the catalysts were evaluated by FTIR spectroscopy with pyridine (Py) as a probe molecule. The catalysts were pressed in self-supporting discs and activated in the IR cell attached to a vacuum line overnight at 400 °C. The adsorption of Py was performed at 250 °C for 1 h. The spectra were recorded using a Perkin Elmer spectrum at room temperature with a resolution of 4 cm^{-1}. The ratio of Brønsted to Lewis acidity was determined based on the method in the literature [33] using Eq. (2).

$$\text{Ratio Bronsted to Lewis acidity} = \frac{A_B \times C_L}{A_L \times C_B} \quad (2)$$

where A_B and A_L are the areas of Brønsted and Lewis acidity from FTIR (cm^{-1}), respectively, C_B is the coefficient of Brønsted acidity (188 cm/mmol) and C_L is the coefficient of Lewis acidity (142 cm/mmol).

2.4. Catalytic runs

The conversion of glucose to levulinic acid was carried out by dissolving 1 g of glucose in 50 ml of distilled water and mixed with 1 g of Fe/HY zeolite catalyst. The solution was heated up in a 100 ml high-pressure reactor at the desired temperature with stirring speed of 200 rpm. After the reaction was completed, the mixture was cooled to room temperature. All samples were filtered before further analysis using HPLC. Randomly selected experimental runs were repeated to test the reproducibility of the data.

2.5. Product analysis

The concentrations of levulinic acid, HMF and formic acid in the liquid product were determined by HPLC (Waters 2690) using column = Hi Plex H; flow rate = 0.6 ml/min; mobile phase 5 mM H_2SO_4, detector = UV 250 nm; retention time = 45 min and column temperature = 60 °C. Standard calibration curves were prepared to assist the determination of the concentration for each respective component. For the analysis of glucose conversion, DNS method was used throughout this study. DNS reagent was prepared by mixing 2 g of NaOH in 100 ml solution. Then, 80 ml of NaOH solution was mixed with 1 g of 3,5-dinitrosalicylic acid, 30 g of potassium sodium tartrate tetrahydrate and 0.83 g of sodium sulfite to produce DNS reagent. One milliliter of supernatant from the product sample was mixed with 4 ml of DNS reagent in a test tube. The resulting solution was heated in boiling water for 5 min. Next, the absorbance of the mixture was measured at 540 nm using UV–Vis spectrophotometer. The glucose concentration of the product was calculated using standard calibration curve of glucose solution with known concentration. Glucose conversion, product yield and selectivity were calculated according to Eqs. (3)–(5):

$$\text{Glucose conversion}\,(\%) = \frac{\text{Initial glucose amount}\,(g) - \text{final glucose amount}\,(g)}{\text{Initial glucose amount}\,(g)} \quad (3)$$

$$\text{Product yeild}\,(\%) = \frac{\text{Product amount}\,(g)}{\text{Initial glucose amount}\,(g)} \times 100\% \quad (4)$$

$$\text{Product selectivity}\,(\%) = \frac{\text{Product yeild}}{\text{glucose conversion}} \times 100\% \quad (5)$$

3. Results and discussion

3.1. Catalyst characterization

3.1.1. Crystallinity and morphology

The XRD patterns of HY and Fe/HY zeolite catalysts are shown in Fig. 2. The peaks observed could be assigned to the FAU structure characterized by intense reflections at 2θ equal to 6.35°, 23.7° and 15.8° [34]. The XRD pattern of the modified HY zeolite completely matched with that of the parent HY zeolite, which indicates that the modification has no obvious effect on the parent zeolite structure. Upon calcination, the Fe species were oxidized and resulted in the formation of iron oxide. The presence of formed iron oxide (Fe_2O_3) along with the HY zeolite could not be observed from XRD patterns. The results are in accordance with previous studies which reported the diffraction lines of Fe_2O_3 could not be observed upon incorporation into the zeolite structure when the iron content was low [35–37] or iron oxide might be present as non-crystalline phase [37]. Besides, good dispersion of Fe species and limited segregation of the oxide particles [36] probably obscured the iron oxide species from being observed with XRD. There was also no significant changes in the number of diffract peaks with respect to HY

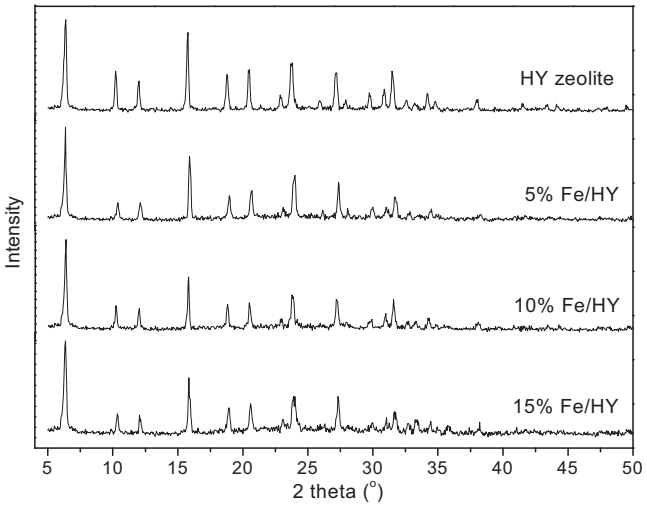

Fig. 2. XRD patterns of HY zeolite and Fe/HY zeolite catalysts.

zeolite, indicating that no crystalline transformation occurred during the impregnation process. Thus, the FAU structure of HY zeolite remained intact for the Fe/HY zeolite catalyst samples.

The calculated crystallite sizes of HY, 5% Fe/HY, 10% Fe/HY and 15% Fe/HY samples are 43.6, 36.8, 35.0 and 33.6 nm, respectively. The average crystallite size of the catalysts were estimated at the highest diffraction peak ($2\theta = 6.35^\circ$) by using Scherrer equation. The crystallite size decreased after impregnation of Fe species on HY zeolite. Similar phenomena were reported when different metals were introduced on porous materials [38–41]. The less intense Fe/HY zeolite XRD peak compared to HY zeolite gave an indication of low crystallinity. Impregnation of Fe on Na-A zeolite also led to decrease in zeolite crystallinity [42]. It is reported that low crystallinity reduced the crystallite size [43]. Partial interaction between Fe species and zeolite framework from the incorporation of Fe to zeolite lattice structure which occurred during the impregnation could probably cause the slight decrease of Fe/HY crystallinity, thus decreasing the crystallite size. Upon modification of HY by impregnation of Fe, the intensity of the characteristic peaks changed without any significant shift of the respective peak positions. The relative crystallinity of Fe/HY zeolite catalysts were calculated based on the integral peak intensity at 2θ (6.35°) with respect to HY zeolite catalyst. The relative crystallinity of 5% Fe/HY, 10% Fe/HY and 15% Fe/HY catalyst are 78, 62 and 56%, respectively. The results demonstrated that the crystallinity of the catalysts reduced after modification, as the presence of Fe could modify the zeolite framework. The decrease in the crystalline structure of the modified HY zeolite catalysts could be due to the strong interaction between the cation (Fe^{3+}) with the oxygen atoms of the alumina tetrahedra in the zeolite framework, where most protons are substituted with Fe during impregnation process. The higher electropositive property of Fe^{3+} might increase the interaction of the cation with the oxygen bond, which weakened the zeolite framework. In addition, the distorted structure of HY zeolite from the impregnated Fe has also reduced the catalyst crystallinity.

The FESEM analyses of the HY and 5% Fe/HY catalysts are exhibited in Fig. 3. The influence of Fe impregnation on the HY zeolite structure can also be confirmed by the FESEM images where small crystallites were observed to be uniformly distributed. FESEM analyses demonstrated that the morphology and particle size of catalysts did not change significantly with Fe impregnation, indicating that no significant crystalline transformation occurred during the modification. Fe_2O_3 was finely dispersed as their presence did not result in significant contrast in the morphology at magnifications up to 22,000×. The EDX result of Fe species has confirmed the impregnation of 5% Fe/HY catalyst. Other elements that have been detected from 5% Fe/HY catalyst by EDX are Si, Al, and O.

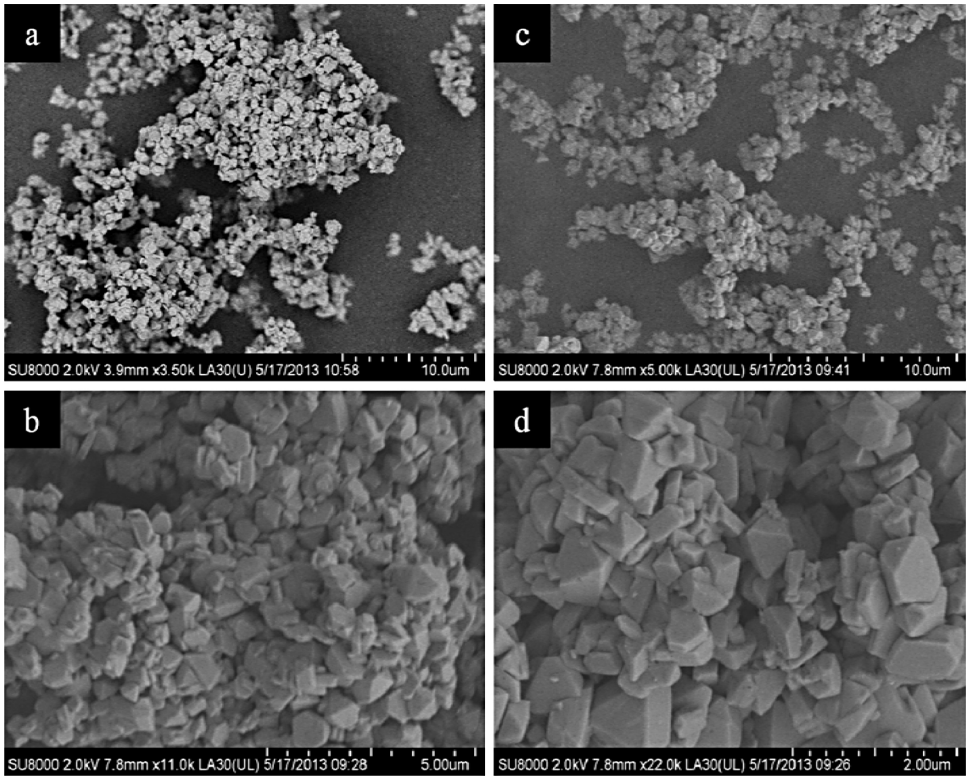

Fig. 3. FESEM of HY zeolite at (a) 3500×, (b) 11,000×, and 5% Fe/HY catalyst at (c) 5000×, (d) 22,000×.

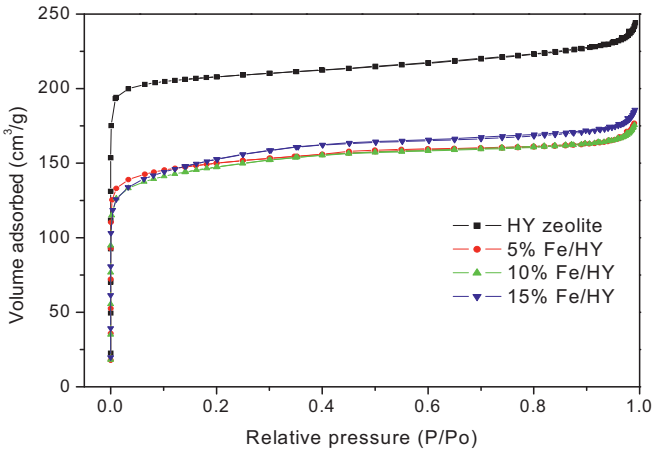

Fig. 4. N_2 adsorption–desorption isotherm of HY zeolite and Fe/HY zeolite catalysts.

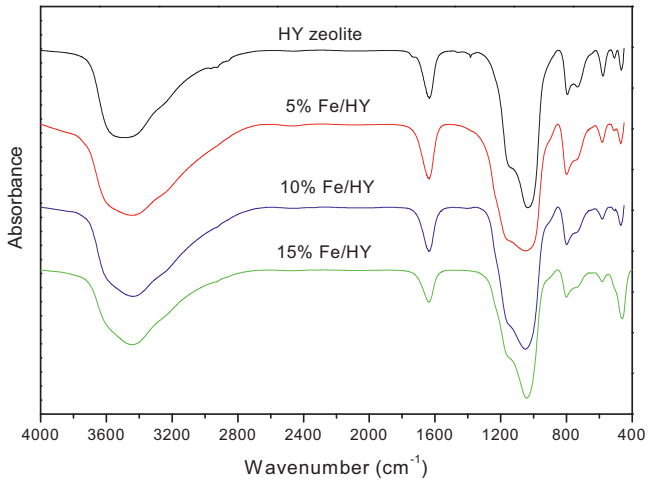

Fig. 5. FTIR spectra of HY zeolite and Fe/HY zeolite catalysts.

3.1.2. Surface are and porosity

The textural properties of HY and Fe/HY zeolite catalysts were studied using N_2 gas physisorption measurement. Fig. 4 displays the N_2 adsorption and desorption isotherms of the catalysts. It was found that all the tested materials exhibited type I isotherm, indicating the microporosity of the materials. The adsorbed gas increased linearly with pressure at very low P/Po. At higher P/Po, the slope of the isotherm decreased progressively with the increase of gas pressure, which is related to the monolayer adsorption on the surface. The surface area, pore volume and pore size of parent HY and Fe/HY zeolite catalysts are summarized in Table 1. The BET surface area and micropore area inferred that impregnation of Fe on HY zeolite has reduced the area of the Fe/HY zeolite catalysts. This can be verified by the decrease in the micropore surface area and volume of the catalysts after impregnation. These effects may be attributed to the presence of Fe_2O_3 and extra framework aluminum species in the interior of the zeolite pores and channels, which could have blocked some of the catalyst pores. The same phenomena have also been reported for the impregnation of different metals: Co, Ni and Cr, on HY zeolite [32,34]. Y-type zeolite consisted of microporous and mesoporous structures. The mean pore diameter of Fe/HY zeolite catalysts slightly increased probably due to metal oxides blocking the micropores and as a consequence the mean pore diameter was higher since there were excess mesopores available in the catalyst [44]. The hierarchical factor (HF) of the catalysts has also been evaluated in this study, with 15% Fe/HY rendering the highest HF (0.1626), followed by 10% Fe/HY, 5% Fe/HY and HY zeolite catalysts. The HF is expressed as the relative mesopority (S_{meso}/S_{BET}) multiplied by the relative microporosity (V_{micro}/V_{total}) and can be used to classify the catalyst structure hierarchically through the porosity feature [45]. Generally, hierarchical zeolite is designed in order to develop the mesopore surface area without affecting and reducing the micropore volume rigorously [32,46,47]. From the HF, the catalytic performance of a catalyst can be inspected, thus the transport in the catalyst pores can be improved [46,48].

3.1.3. Infrared spectroscopy

In order to investigate the structural properties of HY zeolite and Fe/HY zeolite catalysts, FTIR analyses were carried out in the range of 4000–400 cm^{-1}. From Fig. 5, it can be observed that there was no significant band position shift, which indicated that the impregnation of Fe on HY zeolite did not significantly affect the zeolite structure. This supports the earlier discussion on XRD that the zeolite framework remained intact after modification. Generally, IR spectra of zeolite compounds could be identified by two main regions: 1300–400 cm^{-1} and 4000–3000 cm^{-1} [32]. The first region (1300–400 cm^{-1}) indicated the framework vibration of lattice cell (T-O-T unit; where T is SiO_4 or AlO_4 tetrahedron). The IR spectra of Fe_2O_3 can be detected at 445, 460 and 635 cm^{-1} [49], but from the IR spectra, no indication of iron oxides were observed for all Fe/HY zeolite catalysts. Even if Fe_2O_3 was formed, the amount could be too small to be detected by the FTIR. Besides, these Fe_2O_3 bands could not be clearly detected probably because the bands overlapped with the stronger HY zeolite bands. The second region of HY zeolite compound (4000–3000 cm^{-1}) was attributed to the hydroxyl groups attached to the zeolite structure. The band at 3445 cm^{-1} for all catalyst samples signified the vibrations of Si–OH, Al–OH and H-bonded hydroxyl groups [32,35,49]. This typical band of zeolite

Table 1
Surface area and porosity of HY zeolite and Fe/HY zeolite catalysts.

Catalysts	S_{BET}[a] (m^2/g)	S_{meso}[b] (m^2/g)	S_{micro}[c] (m^2/g)	V_{pores}[d] (cm^3/g)	V_{meso}[e] (cm^3/g)	V_{micro}[f] (cm^3/g)	D_{mean}[g] (nm)	D_{meso}[h] (nm)	D_{micro}[i] (nm)	HF[j]
HY zeolite	829.5	76.4	753.1	0.369	0.082	0.287	1.78	5.86	0.54	0.0716
5% Fe/HY	598.9	122.5	476.5	0.279	0.092	0.187	1.83	4.33	0.53	0.1371
10% Fe/HY	549.3	133.6	415.8	0.265	0.098	0.167	1.89	3.77	0.52	0.1532
15% Fe/HY	522.1	145.0	377.1	0.263	0.109	0.154	1.98	3.62	0.52	0.1626

[a] BET surface area was obtained from N_2 adsorption isotherm.
[b] Surface areas of micropore were obtained from the *t*-plot method.
[c] Surface areas of mesopore were obtained from the *t*-plot method.
[d] Volume of pore was obtained from single point desorption method.
[e] Volume of mesopore = ($V_{pores} - V_{micro}$).
[f] Volume of micropore was obtained from the *t*-plot method.
[g] Average pore size was estimated from the desorption average pore diameter (4 V/A by BET).
[h] Mesopore size was estimated from the BJH desorption average pore diameter (4 V/A).
[i] Micropore size was estimated from the density functional theory (DFT) method.
[j] The hierarchical factor (HF) was determined as (V_{micro}/V_{pores}) × (S_{meso}/S_{BET}).

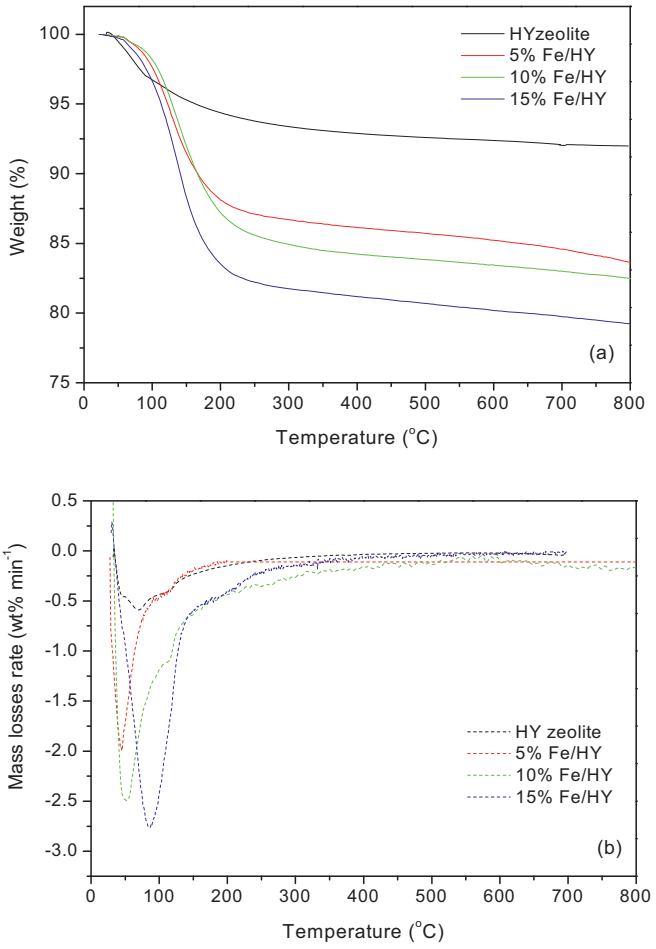

Fig. 6. TG analysis (a) and DTG analysis (b) of HY zeolite, 5% Fe/HY, 10% Fe/HY and 15% Fe/HY catalysts.

at 3445 cm^{-1} indicated the existence of catalytic activity that originated from the acidic sites on the materials [32,44]. The strong IR band within this region strongly signified that the catalyst possesses substantial amount of acid sites, which is essential for the catalytic activity to take place. As observed from the FTIR spectra, the intensity of this band was reduced for all Fe/HY catalysts as Fe cation has interacted with the HY zeolite OH group. Meanwhile, the bands due to the presence of water in zeolite materials resided in the range of 1600–3700 cm^{-1} [50]. The water bending vibration at 1640 cm^{-1} can be observed for all catalysts [35,49].

3.1.4. Thermal gravimetric analysis

The thermal gravimetric analysis of HY and Fe/HY zeolite catalysts as shown in Fig. 6 indicated the mass variations in the catalyst samples from 30 to 800 °C in a heating rate of 10 °C/min. Typical TG curves of the zeolite samples generally indicated two mass variation events [32,34,36]. The first stage in the temperature range of 30–120 °C is attributed to the release of water molecules from the large cavities of the zeolite. The second stage of mass loss took place in the temperature range of 200–800 °C and is assigned to the dehydroxylation of –OH group on the zeolite surface. The mass losses at the temperature range of 30–120 °C was caused by the evaporation of water molecules from the catalyst samples. In the second region, the mass losses are attributed to the thermal dehydroxylation, resulting in the release of HCl gas, the dispersion of Fe on HY zeolite surface in Fe_2O_3 form and the release of aluminum from zeolite framework which probably defect the lattice structure [32]. The defect may be the reason for the decrease in

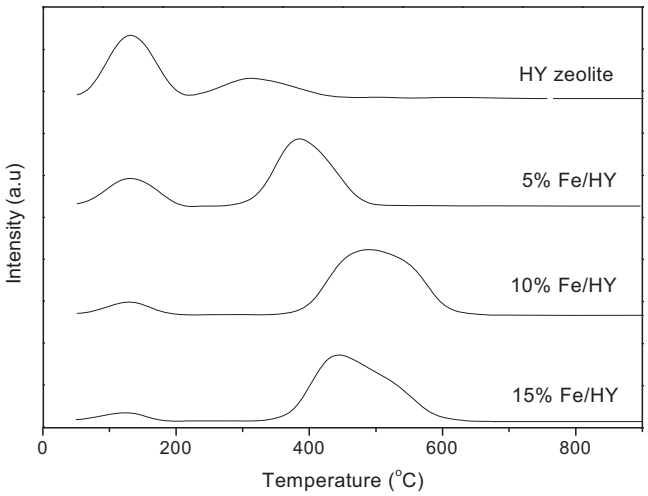

Fig. 7. NH_3-TPD profiles of HY zeolite and Fe/HY zeolite catalysts.

the catalyst relative crystallinity as discussed in the XRD analysis. The catalyst with 15% Fe/HY demonstrated the highest mass losses among all the catalysts tested. Higher mass losses are observed with the increment of $FeCl_3$ loading. As reported previously, if higher temperature range was observed, mass losses over 800 °C might be detected due to the desorption of adsorbed metal from the HY zeolite cage [32,36]. From this analysis, the calcination of the Fe/HY zeolite catalysts is sufficient at 400 °C to validate the interaction of Fe with HY zeolite through the impregnation process.

3.1.5. Acidity

TPD was carried out to evaluate the acidic properties of the catalysts towards the production of levulinic acid. Ammonia (NH_3) was adsorbed on the acid sites of the catalysts due to its basic molecule nature and was removed by thermal desorption process at elevated temperature. The desorption temperature depends on the strength of the interaction between NH_3 and the surface acid sites, and the amount of the desorbed NH_3 were quantified based on the NH_3 desorption peaks [20,32]. The NH_3 desorption peaks can be classified as weak, moderate and strong acid sites based on the desorption temperature of 120–300, 300–500 and 500–700 °C, respectively. The area under the desorption peak indicates the relative number of acid sites present. If the desorption peak area is large, then the number of acid sites is high.

The NH_3-TPD profiles of HY zeolite and Fe/HY catalysts are displayed in Fig. 7. Several desorption peaks existed in all catalysts. The distribution of acid sites for HY zeolite was in accordance with the previous studies [32,51]. HY zeolite exhibited two desorption peaks of ammonia at low and moderate temperatures. It can be observed that all the curves demonstrated a desorption peak around 130 °C, an indication of the weak acid sites present in the catalysts. This range of peak corresponds to weak acid sites from the surface hydroxyl groups, which is consistent with the FTIR result discussed previously. The same trend has also been reported previously [44]. The strength of the acid sites slightly increased when Fe was impregnated into HY zeolite. The desorption peak at higher temperature indicated the stronger acidic sites in the catalyst sample, which suggested that Fe was well diffused on the HY zeolite. From the TPD-ammonia test, it can be inferred that the impregnation of Fe induced new acid sites.

The quantitative data on the acid properties of the catalysts is shown in Table 2. The total acidity of the Fe/HY zeolite catalysts was higher compared to the parent HY zeolite catalyst. All catalysts demonstrated two different desorption peaks: at weak and moderate acid sites. The 5% Fe/HY has the highest total acidity

Table 2
Acidity of HY zeolite and Fe/HY zeolite catalysts.

Catalysts	Weak acidity		Moderate acidity		Total acidity (mmol/g)	Acid sites (μmol/m^2)	Ratio Brønsted to Lewis from IR-Py
	T_d (°C)	Amount (mmol/g)	T_d (°C)	Amount (mmol/g)			
HY zeolite	120	0.92	320	0.66	1.58	1.91	1.51
5% Fe/HY	122	0.55	390	2.26	2.81	4.69	0.39
10% Fe/HY	126	0.38	480	2.30	2.68	4.88	0.29
15% Fe/HY	124	0.14	440	1.98	2.12	4.06	0.07

(2.81 mmol/g) amongst all catalysts tested. The total acidity of 10% Fe/HY and 15% Fe/HY were lower than 5% Fe/HY catalyst although the $FeCl_3$ loading was higher. This is probably due to the presence of Fe_2O_3 covering the acid sites on HY catalyst surface. The same trend has also been reported previously, where metal oxides probably partially covered the acidic sites, thus reducing the catalyst acidity [32,34]. The results demonstrate that the total acidity of the Fe/HY catalysts is not directly related to the amount of Fe loading, but is attributed by the interaction between zeolite and metal oxides in the catalysts. When the acid sites per unit surface area is calculated, the number of acidic sites are 4.88, 4.69 and 4.06 μmol/m^2 for 10% Fe/HY, 5% Fe/HY and 15% Fe/HY catalyst, respectively. It is evident that 10% Fe/HY catalyst comprised of more reactive acid sites compared to the other catalysts in this study.

Infrared spectroscopy of adsorbed Py helped to distinguish between Brønsted and Lewis acid sites of the catalysts as shown in Fig. 8 and the acid sites fraction of the catalysts are as tabulated in Table 2. The Brønsted acid sites can be observed at band 1545 cm^{-1} while the band at 1450 cm^{-1} referred to the Lewis acid sites. In addition, a band at 1490 cm^{-1} was correlated to both Brønsted and Lewis acid sites [32,52]. The intensity of the band assigned to Brønsted acid sites decreased in the following order: HY zeolite, 5% Fe/HY, 10% Fe/HY, 15% Fe/HY and the intensity correlates mainly with the interaction of Fe with the zeolite. The Brønsted acid sites can be generated from the hydroxyl groups and Al framework [53]. Meanwhile, the Lewis acid sites can be detected from the zeolite with defects, amorphous parts and extra framework of Al species. From the spectra, Fe/HY zeolite catalysts exhibited higher Lewis acid sites compared to Brønsted acid sites. The increment of $FeCl_3$ loading resulted in lower Brønsted to Lewis acid ratio.

3.2. Catalytic performance

The catalytic performance of Fe/HY zeolite catalysts was evaluated based on the conversion of glucose to levulinic acid by varying the reaction temperature (120–200 °C) at 180 min reaction time. The reaction time of 180 min was selected for the evaluation of Fe/HY catalysts based on preliminary tests conducted for levulinic acid production using HY zeolite. Meanwhile, the influence of physicochemical properties of the catalysts on the catalytic activity is briefly discussed. Fig. 9a–c depicts the distribution of products from glucose conversion (levulinic acid, formic acid, HMF) using 5% Fe/HY, 10% Fe/HY and 15% Fe/HY catalysts, respectively. Meanwhile, glucose conversion and levulinic acid selectivity are exhibited in Fig. 10. Generally, levulinic acid is the main product from glucose conversion over Fe/HY zeolite catalyst within the determined reaction temperatures. This implies that HMF from the dehydration of glucose feedstock was converted into rehydration products. The presence of water in the system facilitated the HMF rehydration to levulinic acid and formic acid. As reported

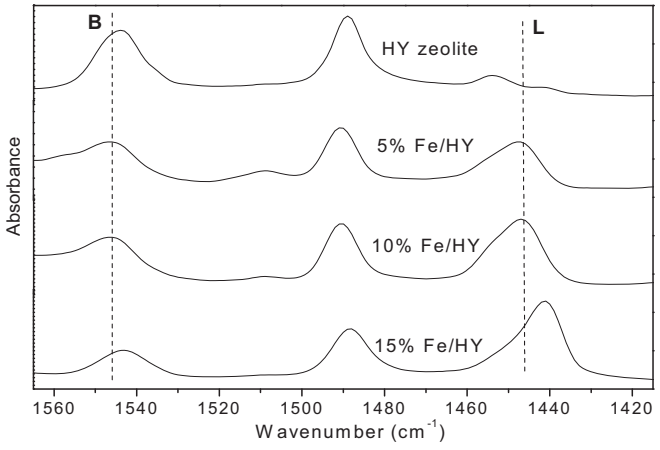

Fig. 8. FTIR spectra of Py adsorbed over HY zeolite and Fe/HY zeolite catalysts.

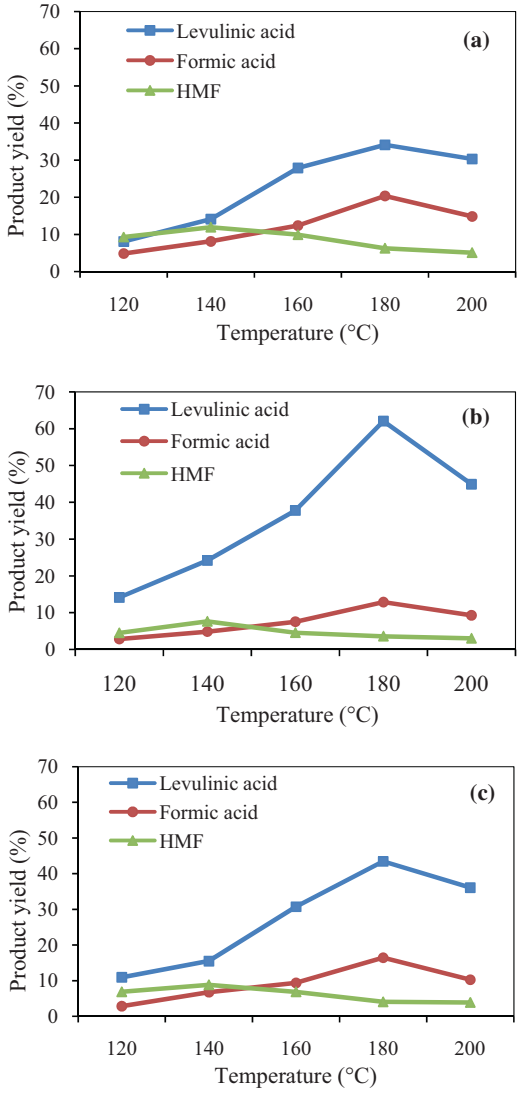

Fig. 9. Product yield versus reaction temperature at 180 min of reaction time for (a) 5% Fe/HY, (b) 10% Fe/HY and (c) 15% Fe/HY catalysts.

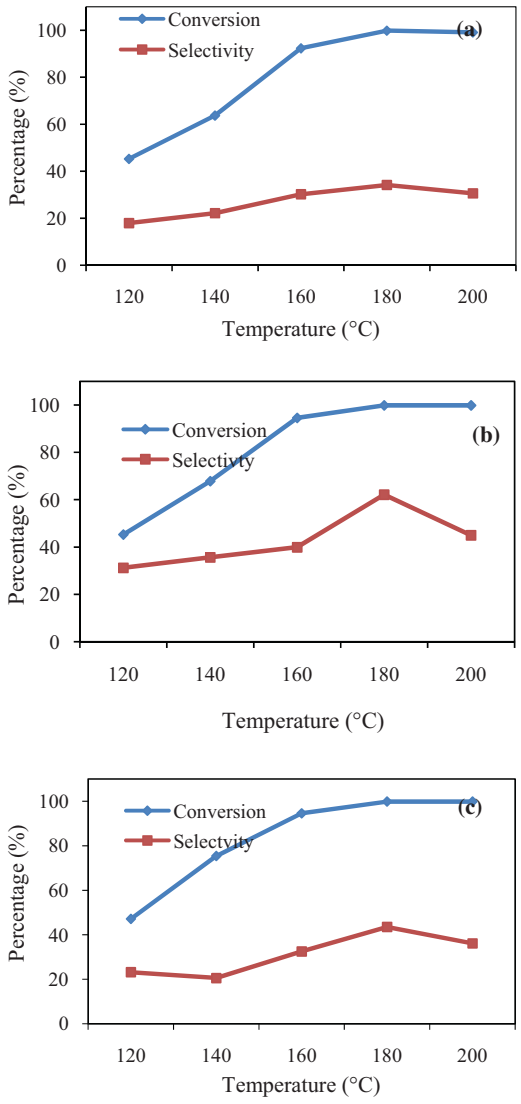

Fig. 10. Glucose conversion and selectivity of levulinic acid versus reaction temperature at 180 min of reaction time for (a) 5% Fe/HY, (b) 10% Fe/HY and (c) 15% Fe/HY catalysts.

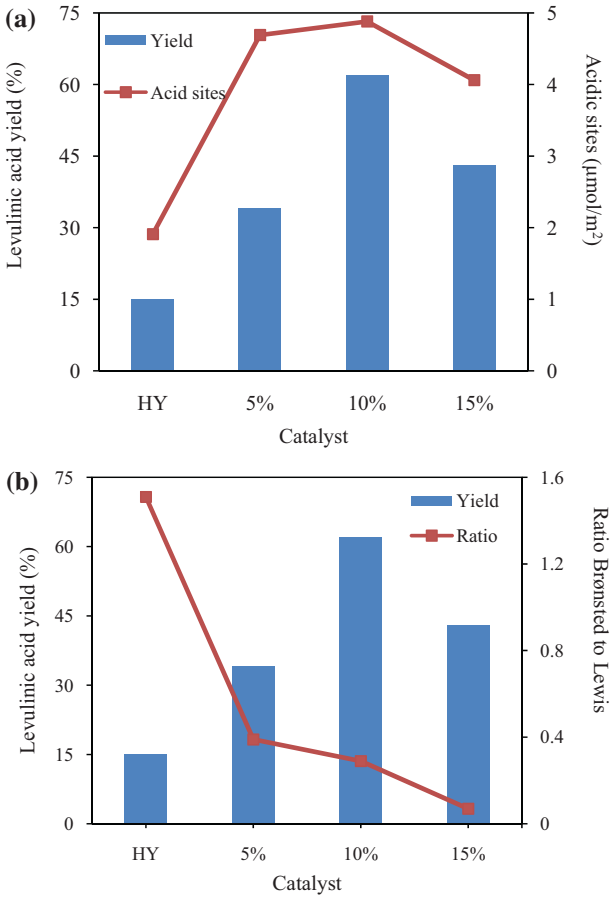

Fig. 11. Levulinic acid yield distribution with acid sites (a) and ratio of Brønsted to Lewis acid sites (b) for HY-HY zeolite, 5–5% Fe/HY, 10–10% Fe/HY and 15–15% Fe/HY catalysts.

previously, HMF was unstable in water which consequently further converted into levulinic acid and formic acid [13]. Theoretically, formic acid produced from HMF rehydration is in equal molar ratio with levulinic acid [18,20]. However, lower formic acid yield compared to levulinic acid yield was observed throughout this study. This condition might be due to the tendency of formic acid to decompose to CO_2, H_2, CO and H_2O in the heat and acidic mediums.

The catalytic performance of Fe/HY zeolite catalysts in glucose dehydration demonstrated that the glucose conversion and levulinic acid yield were enhanced with increasing reaction temperature. At 180 °C, the highest levulinic acid yield was obtained for all the catalysts tested. It is known that elevated temperature can contribute to the acceleration of reaction rate and conversion efficiency. At higher temperature, atoms donate or receive electrons more easily, thus causing a higher chemical reaction rate [10,54]. However, as the temperature increased to 200 °C, lower levulinic acid yield was recorded, probably due to the formation of carbonaceous residue (humin) and deposition of coke on the catalyst surface and pores [55]. The insoluble black solid residues observed in this study was regarded as humins based on previous report [56]. In addition. van Zandvoort et al. [57] experimentally analyzed and confirmed the presence of humins using several analytical techniques after the purification of the humins samples. Complete glucose conversion was achieved at 180 °C. The highest levulinic acid yield and selectivity were obtained from 100% glucose conversion using 10% Fe/HY catalyst (Figs. 9b and 10b). It can be proposed that the product distribution from glucose dehydration relied on the physicochemical properties of the catalyst, which is attributed to acidity, porosity and shape selectivity.

The acid sites of the zeolite catalyst increased after being impregnated with $FeCl_3$. Combined with the catalytic activity testing results, it was found that catalyst acidity influenced the glucose conversion to levulinic acid. Fig. 11 illustrates the relationship between levulinic acid yield and catalyst acidity (acidic sites, ratio of Brønsted to Lewis). It is deduced that 10% Fe/HY catalyst comprised of more reactive acid sites compared to other catalysts in this study. This can be explained by Fig. 11a where the trend of levulinic acid yield from glucose was consistent with the acid sites per unit surface area. The turnover frequency (TOF) for HY, 5% Fe/HY, 10% Fe/HY and 15% Fe/HY are 0.296, 0.349, 0.665 and 0.589 h^{-1}, respectively. The TOF calculations are based on the total concentration of acid sites as determined by NH_3-TPD. On a per site basis, the catalytic activity increased as follows: HY < 5%Fe/HY < 15%Fe/HY < 10%Fe/HY. Therefore, it is comprehensible that acid sites and strength do play a significant role in determining the catalyst activity.

The activity and selectivity of homogeneous and heterogeneous reaction depend on the ratio of Brønsted to Lewis acid sites. Large number of acid sites is essential in all the reaction pathways involved, including isomerization and dehydration/rehydration reaction for levulinic acid production. The isomerization of glucose

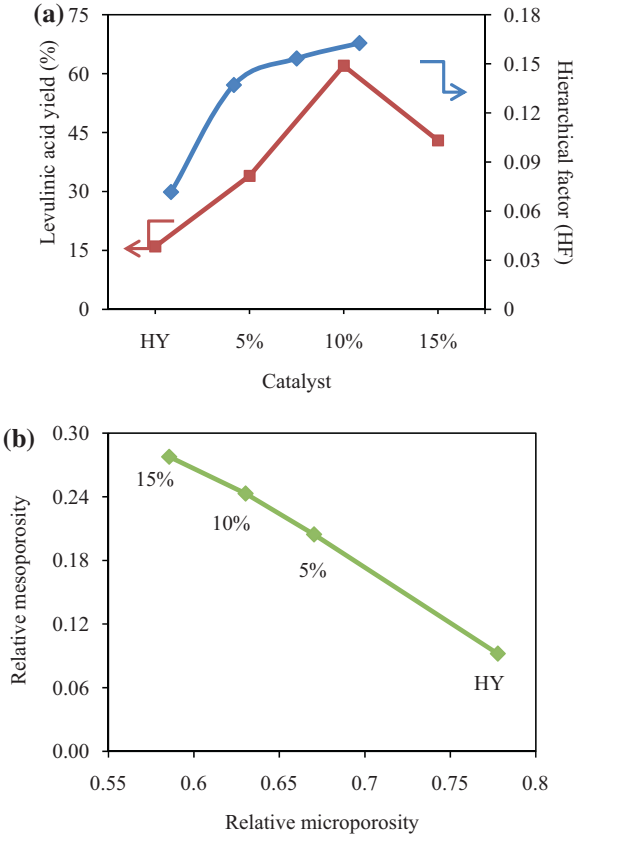

Fig. 12. Levulinic acid yield versus hierarchical factor (a) and relative microporosity versus relative mesoporosity (b), at 180 °C and 180 min of reaction temperature and time for HY–HY zeolite, 5–5% Fe/HY, 10–10% Fe/HY and 15–15% Fe/HY catalysts.

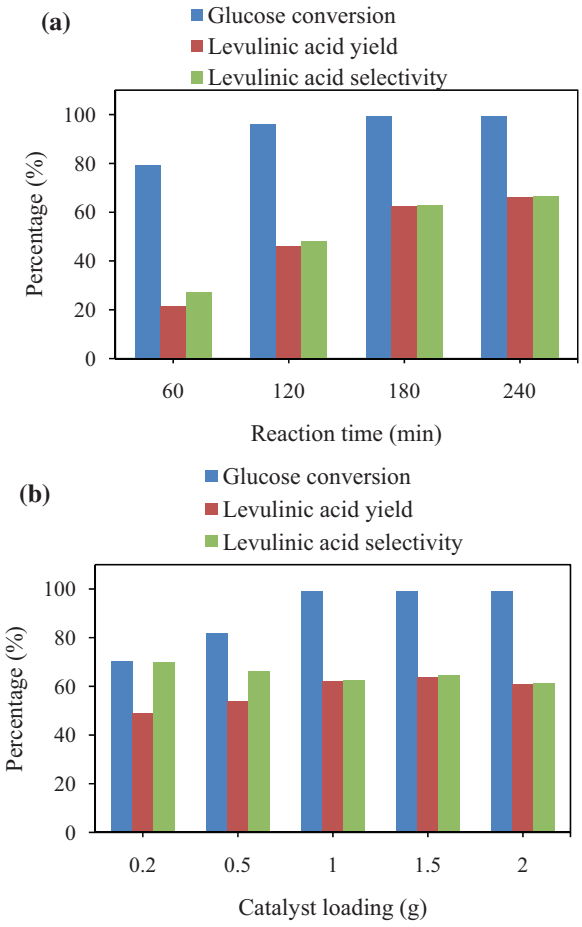

Fig. 13. Effect of reaction time (a) and effect of catalyst loading (b), on glucose conversion, levulinic acid yield and levulinic acid selectivity for 10% Fe/HY catalyst at 180 °C.

into fructose has been reported in favor for Lewis acid sites, whereas the combination of Brønsted and Lewis acidity favor the dehydration/rehydration reaction [28,58–60]. However, the increase in Lewis acid sites can also decrease the levulinic acid production by catalyzing the decomposition of glucose and reaction between glucose and furfural to form humins [28]. It was observed that the levulinic acid production was lower for 15% Fe/HY catalyst compared to the other two Fe/HY zeolite catalysts tested, since 15% Fe/HY possessed higher Lewis acid sites (Fig. 11b). The decrease in the levulinic acid yield from the Fe/HY catalyst at higher Fe loading might be attributed to the formation of other by-product, which is lactic acid. Lactic acid, detected but not quantified in all reaction products, is due to the presence of Lewis acid sites. In previous study, lactic acid has also been detected from the conversion of glucose using a solid metal (IV) phosphate catalysts with the existence of Lewis acid sites [58]. Meanwhile, a thorough study on the direct production of lactic acid from cellulose with solid Lewis acid catalysts has been conducted by Chambon et al. [61].

Besides the acidic property, the effects of catalyst porosity on glucose conversion to levulinic acid should also be taken into consideration (Fig. 12). Few studies have reported that the catalyst pore size has significant influence on the glucose dehydration reactions [20,32]. In the aqueous solutions, catalyst with a large mesopore size allowed the formation of hydronium ion and consequently increased the local protonic acidity. This condition would promote the side reactions including fragmentation and polymerization, thus decreasing the levulinic acid yield [20,62]. This statement can be related to the lowest levulinic acid yield from glucose dehydration over 5% Fe/HY catalyst, which has the highest mesopore size among all the Fe/HY zeolite catalysts tested. The size of mesopores among all the Fe/HY zeolite catalysts were larger than sugar feedstocks (0.9 nm), while the micropore sizes were smaller than the intermediate product, HMF (0.6 nm), which indicated the shape selectivity of the catalysts. From that basis, it is proposed that the dehydration for HMF formation occurred in the mesopores, while the rehydration reaction for levulinic acid formation occurred in the micropores. The shape selective property of Fe/HY zeolite catalysts, which clarified the role of micro- and mesopores for the dehydration/rehydration reaction, can be explained in the proposed reaction mechanism scheme for glucose conversion to levulinic acid.

The HF values plotted against the catalysts with different Fe loading (5, 10, 15%) in Fig. 12a achieved a maximum levulinic acid yield at 10% Fe/HY catalyst, before the loss in micropore volume outweighed the enlargement of external surface. The catalytic performance of the catalysts samples in the levulinic acid production is in good agreement with the HF values. The same trend of result has also been reported by Keller et al. [63] for the condensation of benzaldehyde with melanonitrile using USY385 zeolite catalyst. The changes and variations of hierarchical zeolite catalytic properties could be due to the chemical composition, distribution of acid sites and effects of catalyst surface, which could have influenced the catalytic performance of the respective catalyst [32,45,64]. In this study, large relative mesopority with low relative microporosity advocates higher levulinic acid yield as shown in the results for 10% Fe/HY and 15% Fe/HY catalysts (Fig. 12b). This suggests that the dehydration of glucose to levulinic acid, which consists of glucose isomerization and dehydration to HMF, and also HMF rehydration to levulinic acid requires a

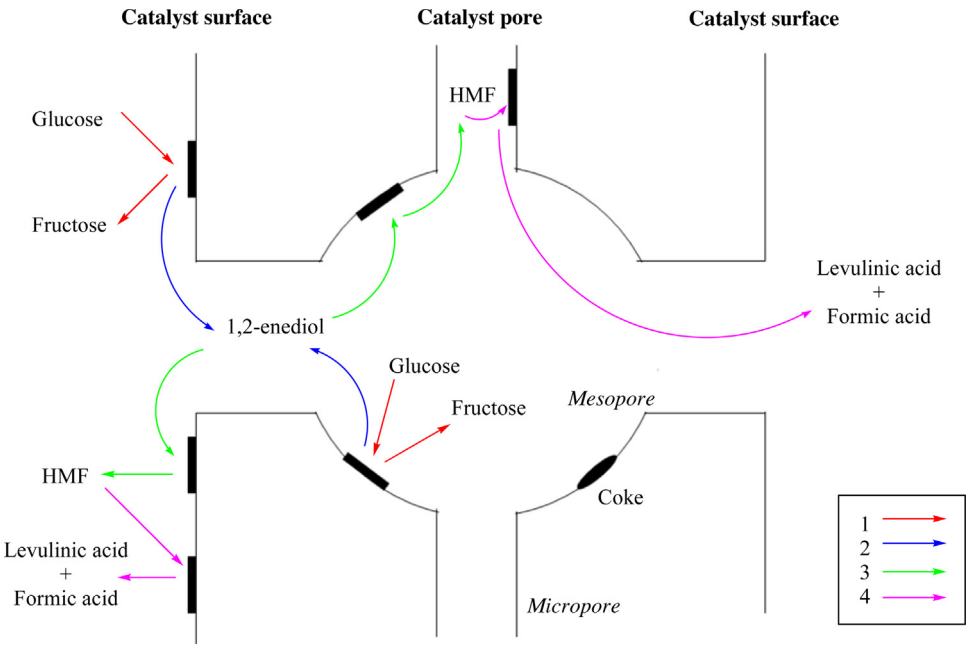

Fig. 14. Proposed reaction mechanism of glucose conversion to levulinic acid over Fe/HY zeolite catalysts. (1) Glucose isomerizes to fructose, (2) monosaccharide ring open to linear chain (1,2-enediol), (3) 1,2-enediol dehydrates to HMF and (4) HMF rehydrates to levulinic acid and formic acid.

catalyst that is mesoporous and microporous with the appropriate pore size.

The experimental results reveal that 10% Fe/HY catalyst gives the highest catalytic performance at 180 °C in a mere 180 min reaction time. Thus, the effect of reaction time was studied using 10% Fe/HY catalyst at 180 °C (Fig. 13a). The results demonstrated that the reaction was quite fast, since after 60 min, 80% glucose conversion was achieved, while for reaction times at 120 min, glucose was almost fully converted. At an appointed catalyst loading, prolonged reaction time was needed for complete conversion of glucose and dehydration/rehydration reaction to levulinic acid. Since the increment in levulinic acid yield was small from 180 to 240 min reaction time, the time 180 min was chosen for the next testing. The levulinic acid yield increased monotonously after 180 min, possibly due to the deposition of residues formed on the catalyst surface that impeded some active sites.

Since catalyst loading affects the glucose conversion, the influence has also been evaluated for loadings between 0.2 and 2 g. Fig. 13b illustrates that glucose conversion and levulinic acid yield increase with loading. On the other hand, maximum levulinic acid selectivity was achieved at a catalyst loading of 0.2 g, but started to decrease beyond this due to the formation of condensation products from the intermediates of glucose with furan products in the aqueous media. This situation might be the consequences of the excess active sites available that boost up hydrolysis process, and at the same time promotes undesired side reactions.

For comparison, both parent catalysts (HY zeolite and $FeCl_3$) were also tested for levulinic acid production from glucose at 180 °C and 180 min. The levulinic acid yield of 16 and 27% were obtained by using the respective catalysts. Based on these findings, it is signified that the modification of HY zeolite by impregnation of $FeCl_3$ exhibited higher catalytic activity towards levulinic acid production compared to the parent catalysts. Both HY zeolite and $FeCl_3$ played an important role in enhancing glucose dehydration to levulinic acid. $FeCl_3$ as Lewis acid has assisted the isomerization of glucose into fructose and facilitated the dehydration and rehydration reaction in producing levulinic acid. The porosity of HY zeolite also affected the whole reaction processes. The same trend of result has also been reported where a large-pore zeolite that contained Lewis acidic $SnCl_4$ facilitated the glucose isomerization/dehydration sequences [65].

3.3. Proposed reaction mechanism

The proposed reaction mechanism of glucose conversion to levulinic acid over Fe/HY zeolite catalyst is shown in Fig. 14. Initially, glucose feedstock isomerized into fructose molecule and these monosachharides rings opened to linear chain in the form of 1,2-enediol. This isomerization and ring opening steps occurred on the catalyst surface and in the catalyst pores over Lewis and Brønsted acid sites [18,19,29]. The sugar feedstock with size smaller than mesopores enhanced the diffusion process into the catalyst pores. It is proposed that pore sizes larger than 1 nm enhanced the sugar diffusion into the catalysts [19,62]. The linear molecule of 1,2-enediol was then dehydrated into HMF over the Lewis acid sites. As proposed by Lourvanij and Rorrer, pore size larger than 1.7 nm was necessary to facilitate the diffusion of HMF away from the active sites [19,62]. In this study, the intermediate product, HMF, was trapped within the micropores since the HMF size was larger than the micropore diameter. HMF could not exit the cage until it was further dehydrated to linear molecules, such as levulinic acid and formic acid. This dehydration process was attributed by the acidic medium at Brønsted sites. Linear molecules, levulinic acid and formic acid were small enough to diffuse out through the pores [18]. The small pore size of the catalyst was sufficient for the conversion of glucose to levulinic acid. This is because larger pore size will increase the local protonic acidity that promotes side reactions, such as fragmentation and polymerization reaction [20]. Besides, larger mesopore size seems to enhance the furfural yield that consequently reduced the levulinic acid yield [62]. Thus, it can be concluded that the catalytic reaction of glucose to levulinic acid was influenced by the acid sites, porous structure and shape selectivity of the catalyst.

3.4. Catalyst reusability

The reusability of solid catalysts is one of the main advantages over liquid catalysts. To evaluate the performance of the former,

Table 3
10% Fe/HY catalyst reusability for glucose conversion to levulinic acid at 180 °C for 180 min reaction time.

Run	Levulinic acid yield (%)	Catalyst recovery (%)
1	62.0	98
2	57.6	97
3	55.7	95
4	49.8	91
5	46.8	88

10% Fe/HY catalyst was selected for levulinic acid production from glucose at 180 °C for 180 min, using 1 g catalyst (for the first cycle), and 1 g glucose. After each catalytic cycle, the catalyst was recovered by centrifugation and washed with water. The catalyst was dried overnight at 120 °C, calcined at 400 °C for 5 h to remove adsorbed by-products, weighed and returned to the subsequent cycles. For the subsequent cycles, the glucose conversion to levulinic acid were conducted at 180 °C, for 180 min, using 1 g of glucose, and the remaining catalyst from the previous cycle. The reusability of Fe/HY zeolite catalyst was examined for five cycles. From the results shown in Table 3, it was determined that the decrease in the levulinic acid yield was less than 15% after five cycles. The loss of catalyst activity may be due to the loss of catalyst powder during the recycling process.

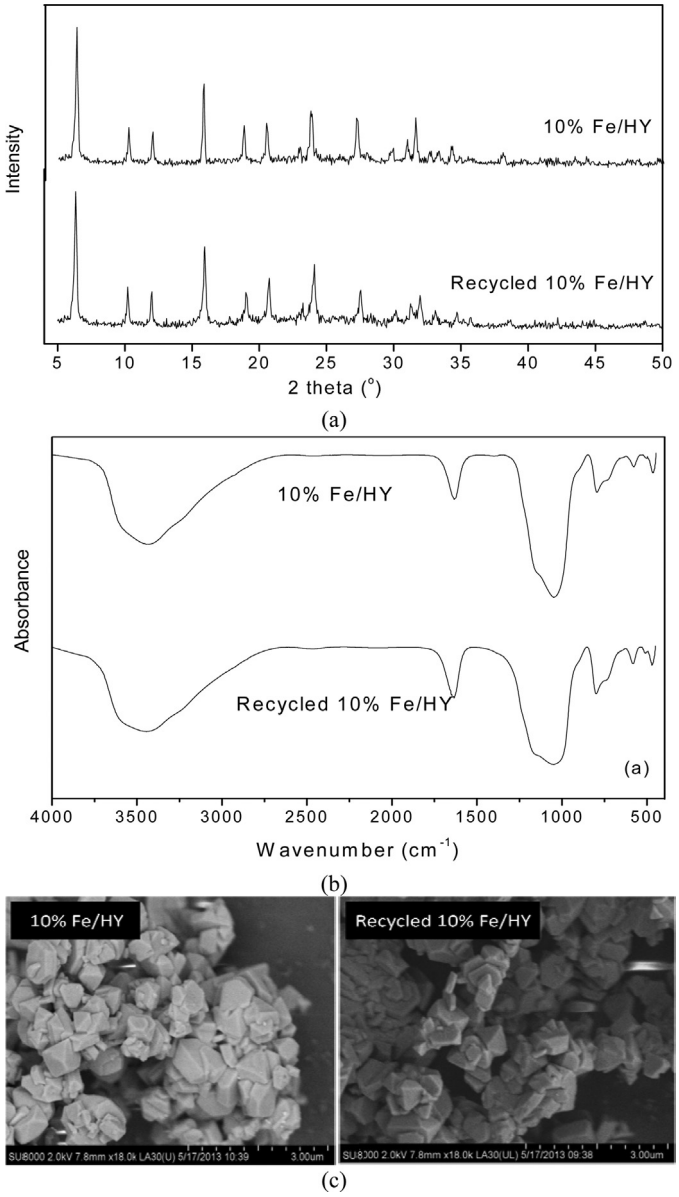

Fig. 15. XRD patterns (a), FTIR spectra (b) and FESEM images (c) of fresh and recycled 10% Fe/HY catalyst.

To study the possibility of Fe leaching from the catalyst into the solution, experimental samples conducted using 10% Fe/HY catalyst at 180 °C for 180 min were subjected to atomic absorption spectroscopy (AAS). The amount of Fe ions was found to be less than 1% of the starting Fe. This infers that the glucose dehydration occurred mainly due to Fe present on the catalyst surface rather than the trace amount of leached Fe ions. The regenerated 10% Fe/HY catalyst has been inspected using XRD, FESEM, N_2 physisorption and FTIR for the comparison with the fresh catalyst (Fig. 15). As shown in Fig. 15a, no significant changes in the diffraction peaks from the XRD profiles were seen after the regeneration, which indicates that the structure of the catalyst sample remained largely undisrupted. FTIR was employed to study the changes of functional groups of the recycled Fe/HY zeolite catalyst (Fig. 15b) and advocated that all the functional groups remain unchanged after the reaction. Similarly, the FESEM images (Fig. 15c) indicate that the external surface of the Fe/HY zeolite particles did not exhibit a significant change in texture after the reaction. Additionally, from the N_2 physisorption analysis, the reduction in surface area for the regenerated catalyst was only 2%.

4. Conclusion

A series of Fe/HY zeolite catalysts comprising of HY zeolite and $FeCl_3$ have been successfully prepared by wet impregnation method. The characterization of Fe/HY zeolite catalysts from XRD and FTIR analyses exhibit the main peaks and bands characteristic of the faujasite Y structure in all samples. Metal impregnation decreases the surface area and volume due to reduced accessibility to micropores. Impregnation of Fe ions distributes Fe_2O_3 inside the zeolite pores. The TPD profiles demonstrate two peaks for NH_3 desorption for all samples, while Fe/HY catalysts exhibit higher acid site density. Lewis acid sites also increase after modification of HY zeolite. The incorporation of Fe in HY zeolite promotes the catalytic activity towards the synthesis of levulinic acid from glucose under mild conditions, with the highest catalytic performance is observed for 10% Fe/HY catalyst. Experimental results verify that the amount of acid sites, ratio of Brønsted to Lewis acid sites, surface area and porosity influence the catalyst activity. Besides, catalytic activity of glucose conversion over the catalysts has a linear dependence with their HF particularly for the catalyst with high crystallinity. Additionally, the Fe-modified HY zeolite catalyst can be reused for at least five times with the activity loss lower than 15%. Characterization of the recycled Fe/HY catalyst manifests that there is insignificant structural change as scrutinized by XRD, FTIR, FESEM and N_2 physisorption.

Acknowledgements

The authors would like to express their sincere gratitude for the financial support received from Universiti Teknologi Malaysia under the Research University Grant (RUG) vote number 02H75. One of the authors (N.A.S.R.) would like to thank the Ministry of Higher Education (MOHE) for MyBrain15 fellowship. We would also like to thank Prof. Dr. Salasiah Endud, Department of Chemistry, Faculty of Science, Universiti Teknologi Malaysia, for the IR-Pyridine characterization.

References

[1] A.M.R. Galletti, C. Antonetti, V.D. Luise, D. Licursi, N.N.o.D. Nasso, BioResources 7 (2012) 1824–1835.
[2] D.M. Alonso, J.Q. Bond, J.A. Dumesic, Green Chemistry 12 (2010) 1493–1513.
[3] M. Yabushita, H. Kobayashi, A. Fukuoka, Appl. Catal. B: Environ. 145 (2014) 1–9.
[4] J.J. Bozell, L. Moens, D.C. Elliott, Y. Wang, G.G. Neuenscwander, S.W. Fitzpatrick, R.J. Bilski, J.L. Jarnefeld, Resources, Conserv. Recycl. 28 (2000) 227–239.
[5] D.R. Fernandes, A.S. Rocha, E.F. Mai, C.J.A. Mota, V. Teixeira da Silva, Appl. Catal. A: Gen. 425–426 (2012) 199–204.
[6] J.C. Serrano-Ruiz, A. Pineda, A.M. Balu, R. Luque, J.M. Campelo, A.A. Romero, J.M. Ramos-Fernández, Catal. Today 195 (2012) 162–168.
[7] D.J. Hayes, S. Fitzpatrick, M.H.B. Hayes, J.R.H. Ross, Biorefineries-Industrial Processes and Products, Wiley-VCH Verlag GmbH, 2008, pp. 139–164.
[8] B. Girisuta, B. Danon, R. Manurung, L.P.B.M. Janssen, H.J. Heeres, Bioresour. Technol. 99 (2008) 8367–8375.
[9] L. Kupiainen, J. Ahola, J. Tanskanen, Chem. Eng. Res. Des. 89 (2011) 2706–2713.
[10] C. Chang, P. Cen, X. Ma, Bioresour. Technol. 98 (2007) 1448–1453.
[11] L. Yan, N. Yang, H. Pang, B. Liao, CLEAN–Soil, Air, Water 36 (2008) 158–163.
[12] Z. Sun, M. Cheng, H. Li, T. Shi, M. Yuan, X. Wang, Z. Jiang, RSC Adv. 2 (2012) 9058–9065.
[13] L. Peng, L. Lin, J. Zhang, J. Zhuang, B. Zhang, Y. Gong, Molecules 15 (2010) 5258–5272.
[14] J. Hegner, K.C. Pereira, B. DeBoef, B.L. Lucht, Tetrahed. Lett. 51 (2010) 2356–2358.
[15] J. Potvin, E. Sorlien, J. Hegner, B. DeBoef, B.L. Lucht, Tetrahed. Lett. 52 (2011) 5891–5893.
[16] X.C. Yu, D.L. Sun, X.S. Li, Asian J. Chem. 22 (2010) 7113–7122.
[17] H. Chen, B. Yu, S. Jin, Bioresou. Technol. 102 (2011) 3568–3570.
[18] J. Jow, G.L. Rorrer, M.C. Hawley, D.T.A. Lamport, Biomass 14 (1987) 185–194.
[19] K. Lourvanij, G.L. Rorrer, Ind. Eng. Chem. Res. 32 (1993) 11–19.
[20] W. Zeng, D.-g. Cheng, H. Zhang, F. Chen, X. Zhan, Reac. Kinet. Mech. Catal. 100 (2010) 377–384.
[21] Y. Liu, L. Lin, X.Y. Sui, J.P. Zhuang, C.S. Pang, Appl. Mech. Mater. 260–261 (2012) 1206–1209.
[22] J. Jae, G.A. Tompsett, A.J. Foster, K.D. Hammond, S.M. Auerbach, R.F. Lobo, G.W. Huber, J. Catal. 279 (2011) 257–268.
[23] N.M. Xavier, S.D. Lucas, A.P. Rauter, J. Mol. Catal. A: Chem. 305 (2009) 84–89.
[24] M. Tan, L. Zhao, Y. Zhang, Biomass Bioenergy 35 (2011) 1367–1370.
[25] Z. Yuan, C. Xu, S. Cheng, M. Leitch, Carbohyd. Res. 346 (2011) 2019–2023.
[26] L. Hu, Y. Sun, L. Lin, Ind. Eng. Chem. Res. 51 (2011) 1099–1104.
[27] L. Mao, L. Zhang, N. Gao, A. Li, Green Chem. 15 (2013) 727–737.
[28] R. Weingarten, G.A. Tompsett, W.C. Conner Jr., G.W. Huber, J. Catal. 279 (2011) 174–182.
[29] I. Agirrezabal-Telleria, I. Gandarias, P.L. Arias, Catal. Today 234 (2014) 42–58.
[30] F. Tao, H. Song, L. Chou, ChemSusChem 3 (2010) 1298–1303.
[31] Z. Zhang, Z.K. Zhao, Carbohyd. Res. 344 (2009) 2069–2072.
[32] N. Ya'aini, N.A.S. Amin, S. Endud, Microporous Mesoporous Mater. 171 (2013) 14–23.
[33] C.A. Emeis, J. Catal. 141 (1993) 347–354.
[34] A.M. Garrido Pedrosa, M.J.B. Souza, D.M.A. Melo, A.S. Araujo, Mater. Res. Bull. 41 (2006) 1105–1111.
[35] S. Turapan, P. Kongkachuichay, P. Worathanakul, Procedia Eng. 32 (2012) 191–197.
[36] L. Li, Q. Shen, J. Li, Z. Hao, Z.P. Xu, G.Q.M. Lu, Appl. Catal. A: Gen. 344 (2008) 131–141.
[37] S. Shwan, J. Jansson, L. Olsson, M. Skoglundh, Catal. Sci. Technol. 4 (2014) 2932–2937.
[38] M. Tahir, N.S. Amin, Appl. Catal. A: Gen. 467 (2013) 483–496.
[39] M. Lashdaf, M. Tiitta, T. Venäläinen, H. Österholm, A.O.I. Krause, Catal. Lett. 94 (2004) 7–14.
[40] S. Hajimirzaee, M. Ainte, B. Soltani, R.M. Behbahani, G.A. Leeke, J. Wood, Chemical Engineering Research and Design.
[41] M. Tahir, N.S. Amin, Appl. Catal. B: Environ. 142–143 (2013) 512–522.
[42] S.-K. Lee, Y.-N. Jang, I.-K. Bae, S.-C. Chae, K.-W. Ryu, J.-K. Kim, Mater. Trans. 50 (2009) 2476–2483.
[43] J. Ma, D. Weng, X. Wu, Z. Si, Z. Wu, Progr. Nat. Sci.: Mater. Int. 23 (2013) 493–500.
[44] Z.Y. Zakaria, J. Linnekoski, N.A.S. Amin, Chem. Eng. J. 207–208 (2012) 803–813.
[45] D. Verboekend, J. Perez-Ramirez, Catal. Sci. Technol. 1 (2011) 879–890.
[46] J. Zheng, Q. Zeng, Y. Yi, Y. Wang, J. Ma, B. Qin, X. Zhang, W. Sun, R. Li, Catal. Today 168 (2011) 124–132.
[47] Z. Xue, T. Zhang, J. Ma, H. Miao, W. Fan, Y. Zhang, R. Li, Microporous Mesoporous Mater. 151 (2012) 271–276.
[48] F. Thibault-Starzyk, I. Stan, S. Abelló, A. Bonilla, K. Thomas, C. Fernandez, J.-P. Gilson, J. Pérez-Ramírez, J. Catal. 264 (2009) 11–14.
[49] Z. Jing, Mater. Lett. 60 (2006) 2217–2221.
[50] H. Hassan, B.H. Hameed, Desalination 276 (2011) 45–52.
[51] S.M. Aboul-Fotouh, Acta Chim. Slovenica 51 (2004) 293–304.
[52] S. Triwahyono, T. Yamada, H. Hattori, Appl. Catal. A: Gen. 242 (2003) 101–109.
[53] M. Niwa, N. Katada, K. Okumura, Characterization and Design of Zeolite Catalysts: Solid Acidity Shape Selectivity and Loading Properties, Springer, Belin, 2010.
[54] Q. Fang, M.A. Hanna, Bioresour. Technol. 81 (2002) 187–192.
[55] C.-H. Zhou, X. Xia, C.-X. Lin, D.-S. Tong, J. Beltramini, Chem. Soc. Rev. 40 (2011) 5588–5617.
[56] H. Cai, C. Li, A. Wang, G. Xu, T. Zhang, Appl. Catal. B: Environ. 123–124 (2012) 333–338.
[57] I. van Zandvoort, Y. Wang, C.B. Rasrendra, E.R.H. van Eck, P.C.A. Bruijnincx, H.J. Heeres, B.M. Weckhuysen, ChemSusChem 6 (2013) 1745–1758.
[58] R. Weingarten, Y.T. Kim, G.A. Tompsett, A. Fernández, K.S. Han, E.W. Hagaman, W.C. Conner Jr., J.A. Dumesic, G.W. Huber, J. Catal. 304 (2013) 123–134.
[59] I. Jiménez-Morales, A. Teckchandani-Ortiz, J. Santamaría-González, P. Maireles-Torres, A. Jiménez-López, Appl. Catal. B: Environ. 144 (2014) 22–28.
[60] I. Jiménez-Morales, M. Moreno-Recio, J. Santamaría-González, P. Maireles-Torres, A. Jiménez-López, Appl. Catal. B: Environ. 154–155 (2014) 190–196.
[61] F. Chambon, F. Rataboul, C. Pinel, A. Cabiac, E. Guillon, N. Essayem, Appl. Catal. B: Environ. 105 (2011) 171–181.
[62] J.S. Kruger, V. Nikolakis, D.G. Vlachos, Curr. Opin. Chem. Eng. 1 (2012) 312–320.
[63] T.C. Keller, S. Isabettini, D. Verboekend, E.G. Rodrigues, J. Perez-Ramirez, Chem. Sci. 5 (2014) 677–684.
[64] D. Verboekend, J.C. Groen, J. Pérez-Ramírez, Adv. Funct. Mater. 20 (2010) 1441–1450.
[65] M. Moliner, Y. Román-Leshkov, M.E. Davis, Proc. Natl Acad. Sci. USA 107 (2010).